Time-of-Flight Secondary Ion Mass Spectrometry of Matrix-Diluted Oligo- and Polypeptides Bombarded With Slow and Fast Projectiles: Positive and Negative Matrix and Analyte Ion Yields, Background Signals, and Sample Aging

Klaus Wittmaack and Wilfried Szymczak
GSF-National Research Center for Environment and Health, Institute of Radiation Protection, Neuherberg, Germany

Gerald Hoheisel and Wilfried Tuszynski
Department of Physics, Carl von Ossietzky University, Oldenburg, Germany

Human angiotensin II, chain B of bovine insulin, and porcine insulin were determined by time-of-flight secondary ion mass spectrometry under impact of ~25 keV Xe^+ and SF_5^+ ion beams and ~100 MeV ^{252}Cf fission fragments. Matrix-embedded samples, dissolved in a large surplus of α-cyano-4-hydroxycinnamic acid, were prepared by nebulizer spray deposition, neat samples by the droplet technique. It is shown that the status of the sample can be assessed by evaluating the matrix-specific features of the mass spectra. The beneficial effect of matrix isolation was small for angiotensin but large for the insulin samples, which did not show parent peaks from neat material. Negative ion yields under SF_5^+ impact were up to a factor of 50 higher than with Xe^+. For positive secondary ions, the enhancement was much smaller. The mass spectra produced by slow ion beams or fast fission fragments were qualitatively similar. Quantitative differences include the following: with fast projectiles the yields were about 10–30 times higher than with slow ions, but similar for negative ion emission under SF_5^+ bombardment; the analyte-to-matrix yield ratios were higher with slow ions and up to 250 times higher than the molar analyte concentration; for analyte ions the peak-to-background ratios were higher using slow projectiles; the fraction of carbon-rich collisionally formed molecular ions was much higher with fast projectiles. Sample aging in vacuum for up to five weeks strongly reduced the yield of protonated analyte molecules ejected by slow ion impact, but not of deprotonated species. Hence protonation seems to correlate with sample "wetness" or the presence of volatile proton-donating additives. (J Am Soc Mass Spectrom 2000, 11, 553–563) © 2000 American Society for Mass Spectrometry

The concept of "matrix assistance" constitutes one of the most promising recent breakthroughs in the mass spectrometry of (nonvolatile) biomolecules. The method became very popular through a discovery by Karas et al. [1] in laser desorption mass spectrometry (LDMS) who found that the high threshold irradiance of certain classes of organic molecules, resulting from poor photon absorption, can be overcome by mixing with material featuring a high molar absorptivity. The initial observations led to the idea and the successful demonstration that nonabsorbing molecules become accessible to LDMS if they are embedded in a resonantly absorbing matrix [2]. Fundamental aspects of the technique, which is now known as matrix-assisted laser desorption/ionization mass spectrometry (MALDI-MS), have been discussed in some detail [3, 4]. Commonly employed MALDI matrices are, for example, 2,5-dihydroxybenzoic acid (2,5-DHB) and α-cyano-4-hydroxycinnamic acid (4HCCA) [5, 6]. Proteins with masses exceeding 10^5 u can be analyzed as a matter of routine and synthetic polymers [7] and nucleic acids [8] have also been identified by MALDI-MS. Even human IgM with a mass close to 10^6 u could be detected as singly charged ions [9]. Applications with emphasis on protein analysis [10] and characterization of synthetic organic polymers [11] were reviewed recently.

By the time of the invention of MALDI, the idea of

Address reprint requests to K. Wittmaack, GSF, Geb. 36, 85758 Neuherberg, Germany. E-mail: wittmaack@gsf.de

1044-0305/00/$20.00
PII S1044-0305(00)00110-0

Received January 27, 2000
Accepted February 14, 2000

matrix assistance had already been applied successfully in secondary ion mass spectrometry (SIMS). Liu et al. [12] showed that the capabilities of SIMS are enhanced if the organic sample is mixed with ammonium chloride. Barber et al. [13, 14] pioneered the use of a liquid glycerol matrix in an approach that was referred to as fast atom bombardment (FAB)-SIMS (an improved terminology has been suggested by Sundqvist [15]). [The improved terminology proposed by Sundqvist reflects the physics of the bombardment and erosion process, the status of the sample, the speed of extraction, and the type of spectrometer. Unfortunately, the suggestions have not been adapted by the scientific community. In this paper we will use a simplified version of Sundqvist's proposal with SIMS as the generic term for secondary ion mass spectrometry induced by swift-particle bombardment. Predominant excitation by nuclear or electronic energy deposition will be specified by the notions "keV/u" or slow ion impact and "MeV/u" or fast ion impact, respectively. The type of spectrometer may be added, e.g., "TOF", "quad" (for a quadrupole-based instrument) or "magnetic" (for magnetic spectrometer).] Liquid matrices can be analyzed by ion bombardment as well [16, 17], provided the sample features sufficient electrical conductivity. Secondary ion emission of small biomolecules from frozen glycerol has also been reported [18].

As an alternative to embedding the analyte material in a suitable matrix, Wolf and Macfarlane [19] successfully used small volatile water insoluble molecules like 9-anthroic acid as substrates for plasma desorption mass spectrometry (PDMS) [20] of biomolecules bombarded with ^{252}Cf fission fragments (MeV/u TOF-SIMS). The main idea behind the *substrate selection* approach was to reduce the internal levels of excitation, to assist ionization, and to achieve more variability in terms of functionality, solubility, hydrophilicity, and volatility of the substrate surface. In related studies using submonolayer quantities of rhodamine 6G deposited on nitrocellulose [21], the Oldenburg group identified interaction between analyte molecules as a limiting factor. Retrospectively, the great success achieved with nitrocellulose as a backing for sample preparation [22] may now be interpreted along the lines of substrate selection.

Successful isolation of analyte molecules has also been achieved by *embedding* oligosaccharides in heteroaromatic compounds [23]. These matrices were found to be suitable for MeV/u TOF-SIMS, and could also be applied for MALDI [24, 25]. The complexity of the phenomena encountered in matrix-assisted MeV/u-SIMS became evident from studies on fullerene samples, either neat or in β-carotine, which showed a yield enhancement for C_{60}^- by a factor of 15 with matrix assistance, but a yield reduction for C_{60}^+ by as much as a factor of 5 [21].

Somewhat surprisingly, keV/u-SIMS has been employed only recently to explore the potential of matrix dilution for the analysis of biomolecules. Wu and Odom [26] reported on a very detailed study into the use of common MALDI matrices for producing parent ions of peptides, proteins, and oligonucleotides with masses up to 10,000 u, using 11 keV Cs^+ primary ions, but the analysis was restricted to positive secondary ions. The mechanism of matrix enhanced secondary ion emission was addressed in qualitative terms, e.g., by concluding [26] that the "matrix dependence is undoubtedly due to the requirement not only that the matrix provides a nestle environment about the analyte molecules and a source of protons for ion formation . . . but also that the matrix/analyte mixture have a sufficiently high concentration of analytes in the top monolayer(s) of the surface."

Clearly, the notion *nestle environment* [26] is less specific than the idea of isolating analyte molecules by adding suitable matrix material [23]. If "gas phase" *proton donation* from the matrix to the analyte were an important factor, one would expect significant differences in yield between positive and negative secondary ions. The aspect of *segregation* of analyte molecules to the sample surface could be invoked in trying to explain differences between keV/u-SIMS and MALDI [26] as well as differences to be expected between keV/u and MeV/u-SIMS. Whereas molecular secondary ions sputtered by keV/u primary ions can only originate from the topmost layers, the ions observed in MALDI or MeV/u-SIMS originate from a larger microvolume.

This study is aimed at further clarifying the mechanism of ion formation in matrix-assisted SIMS by using a strategy that differs significantly from previous approaches.

(1) We concentrated on a single matrix material, i.e., 4HCCA. This material was first used successfully in MALDI [6] and more recent work has shown that reasonable yields may also be obtained in keV/u TOF-SIMS [26]. One reason for choosing 4HCCA is its low vapor pressure which might imply slow aging, even in vacuum. Another property of interest is its low water solubility. 4HCCA-based samples may be cleaned after deposition (and drying) by rinsing with water so that the importance of cationization by attachment of Na may be studied at different stages of surface purity.

(2) To study the correlation between the size or mass of the analyte molecule and the efficiency of matrix isolation we used three different polypeptides with masses differing by almost a factor of 6: Human angiotensin II (molecular weight MW: 1046.2 u), oxidized chain B from bovine insulin (MW: 3495.9 u), and porcine insulin (MW: 5777.6 u).

(3) To assess the importance of different ionization mechanisms, we recorded both positive and negative secondary ion mass spectra at different stages of sample aging.

(4) To explore the effect of the energy deposition process on spectral features and ion yields, we made measurements on essentially the same samples at two vastly different primary ion energies, ~25 keV and ~100 MeV, i.e., under conditions of predominant nu-

clear and electronic excitation, respectively. Such a comparison has been carried out before in conventional organic SIMS [27, 28], but not in matrix-assisted SIMS.

(5) Another novel feature in matrix-assisted SIMS is the use of molecular primary ions. Previous work at GSF on contaminated silicon showed that, in the mass range between 100 and 300 u, negative molecular ion yields produced by SF_5^+ impact are a factor of up to 100 higher than with Xe^+ [29]. Cluster ion impact phenomena were reviewed recently [30], but little is known about yield enhancement from matrix-diluted samples.

(6) Last but not least, we devoted particular interest to the spectral features in the low-mass region dominated by emission from the matrix material. This mass region has been ignored in previous work.

Experimental

The TOF-SIMS instruments used for this work were described before [29, 31]. Only the essential features are summarized here. Both spectrometers feature straight flight tubes without energy focusing so that the mass resolution $m/\Delta m$ is limited to 1000 or less (Δm is the full width at half maximum of a mass peak). This moderate resolution, however, is sufficient for many mass spectrometric studies on biomolecules.

The TOF system at GSF [29], operated at a pressure of about 1×10^{-7} mbar, was coupled to a small accelerator that delivers mass-resolved beams of atomic and molecular ions. The axis of the primary beam line is at 60° to the surface normal of the sample, but the actual angle and energy on impact depend on the target bias and its polarity. In this study, the beam energy was 25 keV, the dc primary ion current typically 1.5 nA, the spot size 400×800 μm^2. The beam was chopped at 10 kHz, with a pulse length of 5 ns. Ejected positive or negative secondary ions were accelerated by a static electric field between a grounded metal grid (transparency 80%, target-to-grid spacing 2 mm) and the target at a bias of (±) 3.5 to 5.5 kV. Near the end of the 60-cm drift tube, the secondary ions were postaccelerated by (±) 6 to 8 kV and then hit a triple microchannel plate detector. The output signals were shaped by a fast discriminator, followed by a multistop time-to-digital converter (TDC, Fast 7886) with a time resolution of 0.5 ns. The mass resolution $m/\Delta m$ was ~250 at m/z of about 1000, partly limited by the pulse width of the (slow) primary ions. Mass spectra for 1.5 to 6×10^6 primary pulses were integrated to get statistically meaningful data (about 50 ions per pulse, data acquisition time typically 5 min, maximum primary ion fluence less than 1×10^{11} ions/cm^2). The spectra shown below are normalized to 1×10^8 incident primary ions, equivalent to 2.4×10^6 pulses at 1.5 nA.

For the detailed comparison of mass spectra intended in this study, reproducibility was of key importance. We have repeatedly measured spectra of the same sample. With very few exceptions related to sample aging (see below) the peak intensities, recorded at the same primary ion charge, were found to be quantitatively the same to within typically ±10%, even in measurements performed on consecutive days. This reflects the high stability of the TOF-SIMS system as well as the very good lateral uniformity of the samples. In part, reproducibility may also be related to the use of a nonfocused primary ion beam with a comparatively large size.

The TOF system at Oldenburg [31] (base pressure 2×10^{-7} mbar) was designed for studies involving desorption of sample material by impact of fission fragments (FFs), i.e., highly charged ions with energies between 80 and 100 MeV. The FFs originate from a ^{252}Cf source (originally 10 μCi) that was centered between the start detector (activated by electrons ejected from a conversion foil) and the sample backing (a 2 μm Mylar foil covered with a 0.2 μm layer of aluminum). The FFs, typically 50 starts/s during the time of these experiments, first passed through the backing and then through the deposited layer of sample material. Positive or negative secondary ions emitted in the forward direction of FF propagation were accelerated in the electric field generated between the target, at a bias of ±18 kV, and a grounded grid (target-to-grid spacing 8 mm). Secondary ion detection and registration hardware were similar to the GSF system ($M/\Delta M \sim 500$). The data for up to several 10^6 start pulses were collected over periods of up to 18 h. The spectra shown below were normalized to 1×10^6 incident FFs.

All analytes and the matrix material were purchased from Sigma-Aldrich Chemie (Deisenhofen, Germany) and applied without further purification. The analytes were dissolved at 1 mg/mL in 0.1% aqueous trifluoroacetic acid, the matrix at 10 mg/mL in acetone. The analyte and matrix solutions were then mixed to get molar matrix-to-analyte-ratios ranging from 500:1 to 2500:1 (human angiotensin II 500:1 [total amount of analyte 10 nmol]; oxidized chain B of bovine insulin 2000:1 [3 nmol]; porcine insulin 2500:1 [2 nmol]). A nebulizer technique developed at Oldenburg [23] was used to produce uniform, presumably microcrystalline layers of sample material by spray depositing 100 μL of the mixed solution on either polished silicon backings or on aluminized Mylar films (for analysis at GSF and Oldenburg, respectively). The thickness of the deposited layers was ~2 μm, the diameter 8 mm. After spraying, the samples were cleaned by rinsing with high-purity water. A few samples were also prepared at GSF by another nebulizer spray technique described recently [32]. The mass spectra of samples prepared by the two spray techniques turned out to be very similar, any differences being largely due to the remaining amount of surface contamination with sodium.

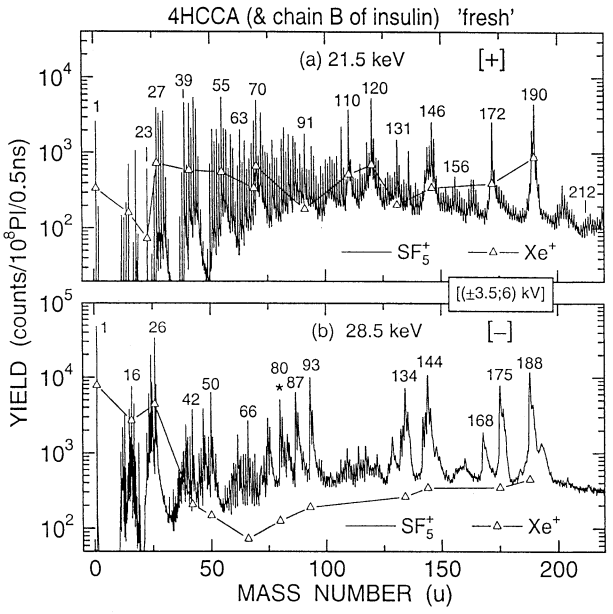

Figure 1. Low-mass region of (**a**) positive and (**b**) negative mass spectra of 4HHCA containing a 1:2000 molar fraction of chain B of insulin. Primary ions SF_5^+, beam energy 25 keV. The target bias and the postacceleration voltage applied to the secondary ions are given in the inset. The open triangles denote the yield of some prominent peaks observed under Xe^+ bombardment. The solid lines are meant to guide the eye. The impact angles in the positive and negative SIMS mode were 69° and 54°, respectively.

Results and Discussion

Matrix-Dominated Mass Region: Slow Ion Impact

Positive and negative secondary ion mass spectra of a mixture of 4HCCA with the chain B of bovine insulin are shown in Figure 1, for mass numbers up to 220 u. The sample is labeled "fresh" to indicate that the spectra were taken at GSF within one to two days after preparation in Oldenburg. The fully drawn spectra relate to SF_5^+ bombardment, the open triangles denote peak intensities recorded under Xe^+ bombardment at the respective masses. Essentially the same spectra have been observed with 4HCCA containing angiotensin or insulin. Only two prominent peaks could be identified that apparently reflect the presence of chain B of insulin as the analyte material, the peaks at *m/z* 80 and 81 in the negative spectrum of Figure 1 (the former marked by an asterisk). The peaks are attributed to SO_3^- and SO_3H^- fragments of the B chain. Otherwise, at *m/z* values up to about 200, the spectra are dominated by emission from the matrix material.

It must be pointed out that the mass spectra in Figure 1 as well as all other spectra shown below constitute raw data in the sense that they have been derived from as-measured spectra (normalized to a common primary ion charge) by merely converting time-of-flight t to mass m or mass number m/z (z is the charge state of the ion). This procedure does not conserve yields in different regions of the spectra because the mass interval δm at m relates to the time interval (bin) δt at the m-equivalent time t as $\delta m \propto \sqrt{m}\delta t$. Corrections are not required if spectral features are discussed only in qualitative terms or if yield changes due to sample aging or a variation in bombardment conditions are studied at certain mass peaks. On the other hand, if yields at different masses are compared in quantitative terms, the $\sqrt{m}$ correction must be applied. Alternatively, signals at the respective mass must be integrated directly in the TOF spectrum.

Returning to Figure 1 we note that, with few exceptions, e.g. in the range from 3 to 11 u, peaks are observed at every unit mass number. The prominent peaks at *m/z* 190 and 188, in the positive and negative ion spectra, respectively, are interpreted as protonated and deprotonated parent ions of 4HCCA, which has the gross structure HO–C_6H_4–CH–C_2N–CO_2H (MW = 189.2 u). The other prominent peaks at *m/z* between 90 and 175 are attributed to fragments of 4HCCA, all containing the benzene ring as the basic element. For example, the peaks at *m/z* 146 and 144 reflect protonated and deprotonated fragments, respectively, after the loss of CO_2. The peak at *m/z* 172 in the positive mode is attributed to the protonated anhydride of the matrix molecule. The peaks observed at *m/z* below about 90, on the other hand, are mostly due to molecular ions that are not reminiscent of the 4HCCA structure. Apparently, these molecules were formed, after the primary ion impact, in fairly energetic, bond-breaking collisions between matrix atoms. Hence "memory" of the original arrangement of atoms in the matrix molecule has been lost. More details are discussed below.

The spectral features observed under SF_5^+ and Xe^+ impact are almost the same and showed little variation across the spray-deposited sample area. The secondary ion yields, however, are much higher for SF_5^+ than for Xe^+. The enhancement factor is significantly higher for negative than for positive ion emission (see also discussion of the high-mass region). In Figure 1 the enhancement factors range from 6 to 8 in the positive mode and from about 10 to 50 in the negative mode. A similar effect has previously been reported for ion emission from contaminated silicon surfaces [29]. Sputtering-yield enhancement of elemental targets due to molecular ion bombardment has been known for many years [33] and may also be expected in the experiments of Figure 1. What is (and was [29]) surprising is the much larger yield enhancement for negative ion emission. A correlation with ion-induced electron emission was tentatively invoked to explain the effect [29], but details of such a mechanism still need to be explored.

Further inspection of Figure 1 shows that there is some additional structure around the mass peaks in the negative mode, panel (b), that is not observed in the positive mode, panel (a). More recent work into this artifact has shown that the "ghost" peaks are due to electrons released by impact of secondary ions on several apertures located along the drift tube of the TOF-SIMS instrument at GSF. A fraction of these elec-

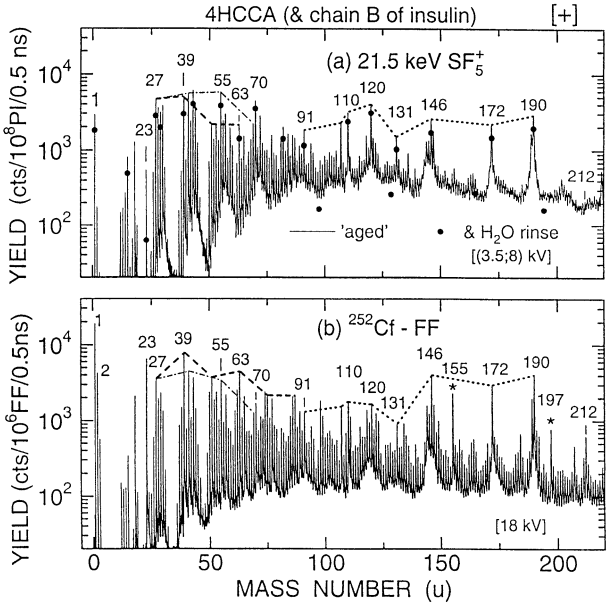

Figure 2. (**a**) The same as Figure 1, but for positive secondary ions recorded after sample storage in vacuum for about five weeks. The solid circles denote peak heights and valleys after an additional rinse with high-purity water. Note the higher postacceleration voltage compared to Figure 1. The meaning of the dashed, dash–dotted, and dotted lines is discussed in the text. (**b**) The same as (**a**), but for a sample bombarded with fission fragments.

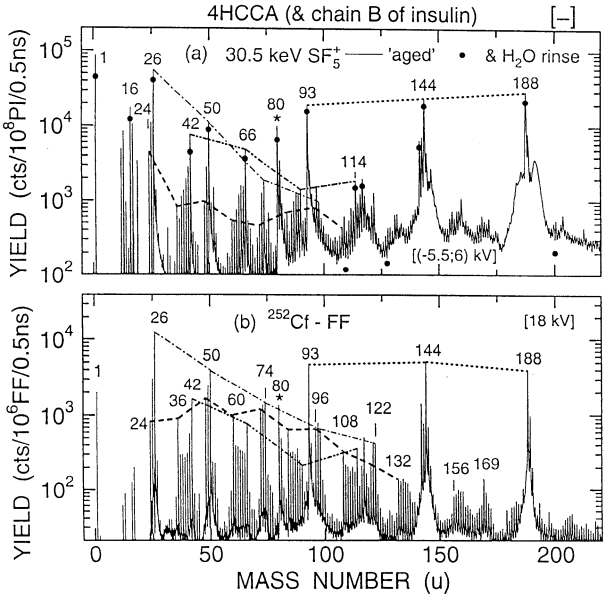

Figure 3. The same as Figure 2, but for negative ions. Note the higher target bias in (**a**) compared to Figure 1b. Impact angle 52°.

trons is attracted to the positively biased detector, where they produce sizable peaks slightly in advance or after the respective secondary ion, with electron arrival times depending on the location and bias potentials of the apertures and the detector. (Meanwhile the spectrometer has been modified significantly to the extent that the relative height of ghost peaks is well below the 1% level.) Although the negative-ion mass spectra recorded in course of the present work at GSF were contaminated by the parasitic electrons, the essential information derived from the spectra was not significantly distorted by this particular artifact.

Another interesting detail observed in the negative spectrum of Figure 1b is the broad feature on the high-mass side of the 4HHCA parent peak at *m/z* 188 which is due to neutrals of the same mass. Separation between neutrals and ions was brought about by the 6-kV postacceleration that had been applied to the detector and a preceding electrode. The peaks corresponding to impact of neutrals have been found to be particularly large for the (unfragmented) parent ions. More detailed studies into this phenomenon are currently underway at GSF.

Positive and negative-ion mass spectra recorded with the same sample as in Figure 1, but after storage for about five weeks in vacuum, are shown in Figures 2a and 3a, respectively. In terms of the relative height of the prominent peaks, the spectra are essentially identical at *m/z* values <100 and very similar at higher masses. It should be noted that the extraction (postacceleration) voltage used in taking the negative (positive)-ion spectra of the aged samples was higher by 2 kV than on the fresh samples. Thereby the secondary ion yields were enhanced, most significantly in the negative spectra above *m/z* 100. In the 4HCCA-dominated mass region, however, "aging" causes a slight loss in peak height of positive secondary ions and a sizable decrease in peak-to-background ratio (at *m/z* > 50). A significantly larger effect of sample aging by storage in vacuum is evident in the negative spectra, cf. Figures 1b and 3a. The rather prominent peaks at *m/z* 87, 134, 168, and 175 in Figure 1b have almost completely disappeared in Figure 3b.

To explore the effect of treatment with water, the aged samples were exposed to air, and a droplet of high-purity water was deposited on the layers for a few minutes. Thereafter the water was removed with a pipette and the samples were transferred back into the vacuum chamber. For a number of prominent peaks, the yields observed after this "H_2O rinse" are denoted by full circles, cf. Figures 2a and 3a. Generally, the yields are reduced by 10%–30%. The only exception is Na^+, in which case the yield was reduced by as much as a factor of 8, cf. Figure 2a. Hence we conclude that exposure to water does in fact reduce the sodium contamination of the sample quite efficiently. The absence of a similarly drastic effect of water on the yield of molecular ions implies that none of the major peaks was formed by attachment of Na^+. In fact, the peak at *m/z* 212, which may be attributed to Na attachment to 4HCCA, is very weak in Figures 1a and 2a.

We did, however, identify a correlation between the ion yields of sodium and all other positively charged ions. Evaluating the spectra of several differently

treated samples, with various levels of sodium contamination before and after cleaning, we found that the yields of atomic and molecular ions, collisionally formed as well as matrix related, scale roughly as the square root of the Na^+ yield. The origin of this correlation is not clear at present. Apparently, the Na^+ yield constitutes some measure of the electronic state of the surface which, in turn, controls the ionization probability of ejected atoms and molecules.

Comparison of Matrix Spectra Due to Slow and Fast Ion Impact

Mass spectra recorded under impact of fission fragments (FF) are depicted in the lower panels (b) of Figures 2 and 3. Comparison with the spectra for SF_5^+ bombardment, shown in the respective upper panels (a), reveals surprising similarities in the relative peak heights, notably in the matrix-dominated mass region. This similarity becomes quite evident from the dotted lines connecting some of the peaks that have been attributed to the emission of intact 4HCCA and fragments thereof (dotted lines in Figures 2 and 3). The main difference in this mass region is the observation of distinct peaks at *m/z* 155 and 197 in the positive FF-induced spectrum in Figure 2b. As these lines do not appear in spectra of 4HCCA containing angiotensin or insulin, we believe that they are due to fragments of the chain B of insulin. The peak at *m/z* 212 in Figure 2b is attributed to cationization of 4HCCA by Na attachment, in accordance with the comparatively high signal of atomic $^{23}Na^+$.

Taking a look at absolute yields, we note that the normalized peak count rates in Figure 2a, b are about the same, but the number of incident primary ions is a factor of 100 higher for SF_5^+ than for FFs. This might be interpreted as a corresponding difference in yield per incident projectile. However, comparison of absolute yields is somewhat difficult because two different instruments were used to acquire the mass spectra (at *m/z* 190, $\delta m/\delta t = 0.077$ and 0.044 u/bin for the measurements with SF_5^+ and FFs, respectively, in Figure 2). As the spectrometer at Oldenburg was operated at a much higher secondary ion extraction voltage (18 kV) than at GSF (3.5–5.5 kV), we expect the former instrument to feature much higher transmission and detection efficiency than the latter. Measurements performed at GSF at different extraction and postacceleration voltages suggest that the yields of molecular ions, with $m/z < 150$, increase roughly as the square root of the impact energy on the detector. Hence the number of positive ions ejected per incident projectile may only be a factor of 10–20 higher for FFs than for SF_5^+. For negative ions this number is even smaller because the (raw) yield difference in Figure 3a, b amounts to a factor of only about 10.

Inspection of the low-mass region ($m/z < 100$) reveals some interesting differences in the relative yields of secondary ions produced by SF_5^+ ions and FFs, i.e., by projectiles of vastly different energies. (i) The yields of H^+, H_2^+, and H_3^+ observed under bombardment with FFs are significantly higher than with SF_5^+. For H^- the behavior is just opposite. The much higher H^+ yield under MeV/u bombardment compared to keV/u has been known for some time [34] and is related to the high charge state of FFs. (ii) The positive secondary ion spectra provide evidence that, under FF bombardment, the collisionally formed carbon-rich C_n-based molecular species are generally emitted with higher abundance than under impact of SF_5^+ (or Xe^+). To illustrate this finding, the peaks in Figure 2 due to the same series of hydrocarbon molecules have been connected by straight lines, e.g., $(CH_2)_nCH^+$ (thin dash–dotted line) and $C_nCH_3^+$, with $n = 1, 2, \ldots$ (thick dashed line). (iii) Similar features are found in the negative spectra, the difference being that hydrocarbon molecules are not (or only with very low yield) emitted as negative ions. Instead, ions of acetylenic structure are observed, as previously reported for MeV-ion impact [35, 36]. The dominant negatively charged molecular ions are found at *m/z* 26 and are attributed to CN^-. The lines connecting prominent peaks in Figure 3 are assumed to be due to $C_{2n}H_2^-$ or $C_{2(n-1)}CN^-$ (thin dash–dotted line), $C_{2n}CNO^-$ (dash–double dotted line), and C_{n+1}^- (thick dashed line). The observed abundant FF-induced emission of carbon-rich molecules provides evidence for a very high density of nuclear excitation along the track of the FFs, even though the initial energy transfer from the FFs to the target takes place primarily via electronic excitation. The deposited energy is converted very efficiently into nuclear motion so that, at a later stage, the central part of the exited volume apparently contains essentially free atoms that combine to form molecules that did not exist as such in the undisturbed sample [35–37]. The relative abundance of the ionized molecules produced in such events will be determined by the amount of excitation, the bond strength, and the ionization probability.

In support of this simple picture, Figure 4 shows mass spectra of neat angiotensin. At *m/z* values <100 the positive-ion spectra are very similar to those observed with 4HCCA, cf. Figures 1a and 2a. The similarity in the negative-ion spectra is not as pronounced, probably because of the difference in the relative abundance of C, N, and O (normalized to carbon, the molecular composition may be written $CH_{0.7}N_{0.1}O_{0.3}$ for 4HCCA and $CH_{1.45}N_{0.28}O_{0.26}$ for angiotensin). At higher masses, the positive and negative-ion spectra in Figure 4 appear to be dominated by fragments of angiotensin. The high Na^+ yield in Figure 4a indicates appreciable sodium contamination, owing to the lack of a cleaning treatment. Some of the prominent peaks seem to reflect the presence of trifluoroacetic acid used for dissolving the analytes. The peak at *m/z* 113, for example, has been attributed to the anion of trifluoracetate [38]. Last but not least, we note that the yield ratio for SF_5^+ vs Xe^+ bombardment amounts to only a factor of 2 to 3 in the

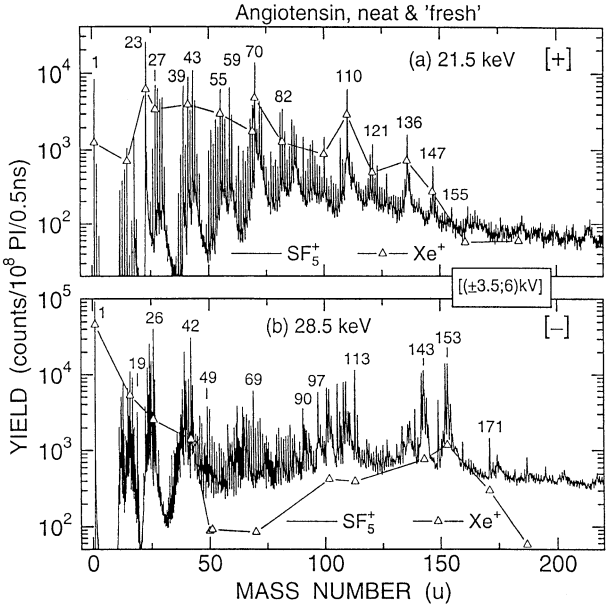

Figure 4. The same as Figure 1, but for neat angiotensin.

positive spectra but to a factor of 20 to 50 in the negative spectra.

Comparison of Spectra and Yields in the High-Mass Region

Turning now to the analysis of the oligo- and polypeptides, we show, in Figure 5, the high-mass sections of the spectra for neat angiotensin II, measured under Xe^+ and SF_5^+ bombardment. The most prominent peaks are due to the protonated and deprotonated parent species [for simplicity the respective peaks in Figures 5–9 are labeled M^+ rather than $(M + H)^+$]. Owing to the large amount of sodium in the sample, identified in Figure 4a,

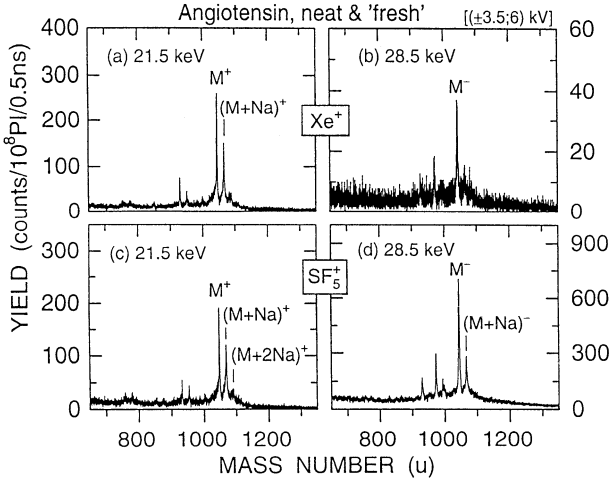

Figure 5. High-mass section of the positive and negative mass spectra of neat angiotensin bombarded with Xe^+, (**a**) and (**b**), and SF_5^+, (**c**) and (**d**).

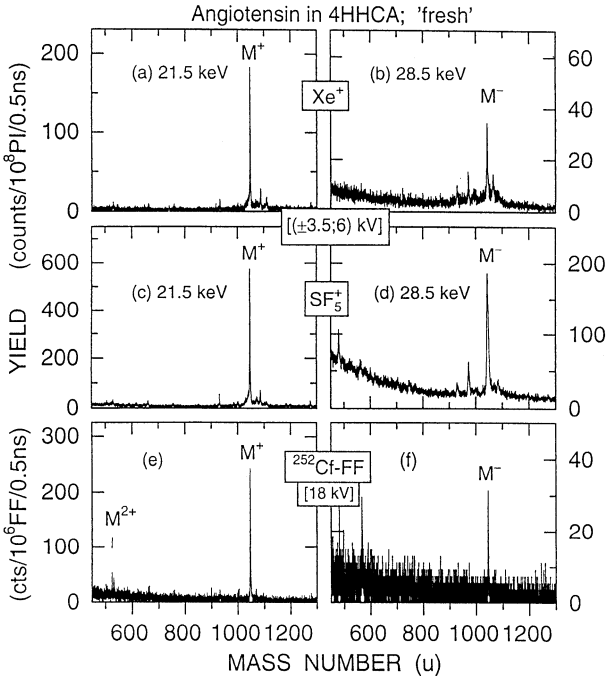

Figure 6. High-mass section of the positive and negative mass spectra of angiotensin in 4HCCA bombarded with Xe^+, (**a**) and (**b**), SF_5^+, (**c**) and (**d**), and fission fragments, (**e**) and (**f**). Spectra (**b**), (**d**), and (**f**) have been passed through a 3-point smooth.

the peaks reflecting attachment of Na are also present with comparatively high intensity, not only in the positive but also in the negative spectra. There are even indications for positive ion formation by double Na exchange. The fragment peak at *m/z* 931 is attributed to the loss of aspartate. The yield enhancement for the negative parent ions, achieved by changing from Xe^+ to SF_5^+ bombardment (Figure 5b, d), shows the same trend as in Figure 4b but is a factor of about 2 smaller than in the matrix-dominated mass region.

Mass spectra for angiotensin embedded in 4HCCA are presented in Figure 6. For Xe^+ bombardment, the yields of the protonated molecules are similar to those observed with neat angiotensin, cf. Figure 5a, b. However, the peak-to-background ratio is distinctly higher (better) with matrix assistance than without, and the fragment peak at *m/z* 931 is much less pronounced. This finding might indicate that the matrix serves to reduce the internal energy of the ejected parent ion. There is no evidence for Na attachment, in accordance with the comparatively low Na^+ yield observed with 4HCCA-embedded analytes, cf. Figure 1a. The SF_5^+/Xe^+ yield enhancement seen in Figure 6, factor ~3 in the positive mode, factor ~6 in the negative mode, is quantitatively different from the effect observed with neat angiotensin. This result indicates that the mechanism of yield enhancement is rather complex.

The mass spectra of 4HCCA-embedded angiotensin II observed under FF bombardment, Figure 6e, f, are very similar to those produced by slow ion impact. To

Table 1. Normalized analyte-to-matrix detection efficiencies observed in the positive and negative SIMS mode under bombardment with slow ions and fast fission fragments (for definition of efficiencies see text)

	Peak efficiency (TOF)			Total (integral) efficiency		
SIMS mode	Xe^+	SF_5^+	FF	Xe^+	SF_5^+	FF
			Human angiotensin II			
+	100	63	34	255	160	107
−	35	8.5	4	105	25	13
+/− ratio	2.9	7.4	8.5	2.4	6.4	8.2
			Chain B of bovine insulin			
+	12.5	8.7	2.5	58	40	19
−	5	5	2.5	38	38	19
+/− ratio	2.5	1.7	1	1.5	1	1
			Porcine insulin			
+	9.6	6.6	4.5	64	50	32

identify differences in the efficiency of producing intact analyte molecules by slow (keV/u) and fast (MeV/u) projectiles, we compare the yields of analyte and matrix parent ions, Y_a and Y_m, respectively. As the matrix ion yields were found to be unaffected by the presence of the analyte in the sample, we can use the results of Figures 1–3 and 6 to determine ratios of background-corrected peak signals for angiotensin in 4HCCA. For Xe^+, SF_5^+, and FF the analyte-to-matrix peak yield ratios, $\hat{r}_{a,m}^{(t)} = \hat{Y}_a^{(t)}/\hat{Y}_m^{(t)}$, turned out to be 0.20, 0.125, and 0.067 in the positive mode and 0.07, 0.017 and 0.0077 in the negative mode. The superscript (t) relates the fact that we are comparing peak yields derived directly from the raw TOF spectra (see discussion with reference to Figure 2). Because peak widths are significantly larger for the analyte ions than for the matrix ions, the (total) analyte-to-matrix yield ratios, $r_{a,m} = Y_a/Y_m$, derived from corrected peak yields, $\hat{Y}_a^{(t)}/\sqrt{m_a}$ and $\hat{Y}_m^{(t)}/\sqrt{m_m}$, times the respective FWHM in the mass spectrum are larger as well: 0.51, 0.32, and 0.21 (positive mode); 0.21, 0.05, and 0.026 (negative mode). These numbers are much larger than the molar analyte-to-matrix concentration ratio, $c_{a,m}$, in the as-prepared sample solution, which was 0.002 for angiotensin in 4HCCA. The high yield ratios become fully evident by normalizing to the molar concentration. The scaled ratios for the peak yields, i.e., $\hat{\epsilon}_{a,m}^{(t)} = \hat{r}_{a,m}^{(t)}/c_{a,m}$, and the equivalent for the total yields will be referred to as the analyte-to-matrix detection efficiencies.

The results for angiotensin in 4HCCA, compiled in Table 1, are quite surprising. (i) In the positive as well as the negative-ion TOF-SIMS mode, analyte molecules are detected much more efficiently than the matrix molecules. The analyte-to-matrix detection efficiencies are particularly large for positive ions, in which case they range between about 100 and 250. This favorable aspect of matrix isolated TOF-SIMS does not seem to have been recognized before. Part of the effect may be due to surface segregation of the analyte. Evidence supporting the idea of segregation comes from studies on the yield of α-cyclodextrin embedded in 3-aminopyridine. Reducing the molar fraction of the analyte by a factor of 100, i.e., from 1:10 to 1:1000, the analyte ion yield decreased by only a factor of 2.3 [23]. More detailed concentration-dependent studies on analyte as well as matrix ion yields are highly desirable to clarify the issue. (ii) In terms of yield ratios and analyte-to-matrix detection efficiencies, Xe^+ is found to be the most efficient projectile in that the number of intact analyte ions ejected per intact matrix ions is largest, for positive as well as for negative ions. (iii) For the yield ratios and efficiencies, an SF_5^+ effect is no longer evident, the reason being that the yield enhancement is larger with matrix ions than with analyte ions. (iv) Somewhat unexpectedly, the analyte-to-matrix yield ratios and detection efficiencies are lowest under impact of FFs (note that the above numbers would be even more in favor of slow ion bombardment if the Xe^+ and SF_5^+ measurements had been carried out at higher extraction and detector voltages).

The reason for the difference in analyte-to-matrix detection efficiency observed with slow and fast projectile impact is not clear at this point. One may speculate that the effect is related to the difference in energy density and excited volume generated at the two vastly different projectile velocities. According to TRIM [39] simulations performed at Oldenburg, the range of 25 keV Xe^+ ions in the matrix material is 26 nm, but only half as large for the constituents of 25 keV SF_5^+. Hence the energy density deposited on impact of SF_5^+ will be significantly larger than with Xe^+. The range of FFs is larger than the sample thickness of about 2 μm, and the energy deposited per unit path length exceeds that of the slow ions by about one order of magnitude. The high-energy (~2 keV) electrons generated by the fast fission fragments along the track have rather long ranges [15], estimated to be as large as 30 to 50 nm. There is common consensus that intact molecules can only be produced at the "quiet" rim of the excited area or volume. The ratio of the quiet rim to the highly agitated core will decrease roughly as the inverse of some adequately defined radius of the excited region. The yield ratios quoted above are in general accordance with this reasoning. The constraints in terms of maximum tolerable energy density are likely to become more severe the larger the ejected molecule. On the

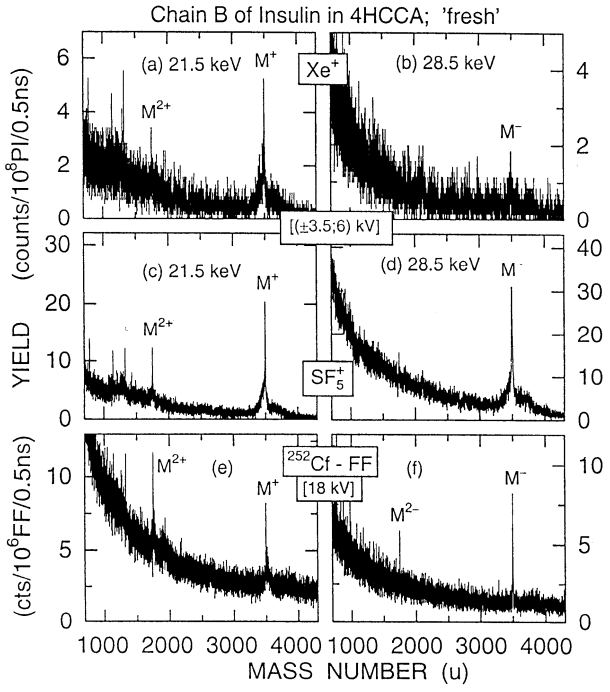

Figure 7. The same as Figure 6, but for chain B of insulin in 4HCCA. 5-point smooth for all spectra.

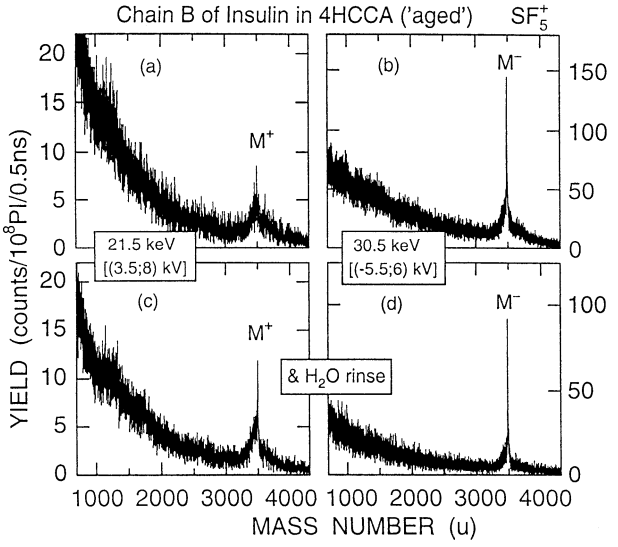

Figure 8. Comparison of mass spectra of chain B of insulin, (**a**) and (**b**) after long-term storage in vacuum and (**c**) and (**d**) after additional rinsing with high-purity water. 5-point smooth for spectra (**a**) and (**c**).

other hand, all arguments are valid only as long as the excited volumes are large enough for the analyte species in question.

Mass spectra for the oxidized chain B of bovine insulin embedded in 4HCCA are shown in Figure 7. The main differences compared to the results for angiotensin II are the lower parent ion yields and the observation of rather strong signals due to doubly protonated analyte molecules (labeled M^{2+}). It is also interesting to note that the analyte peak-to-background ratio for slow ion impact is a factor of about 5 higher (more favorable) than with fast FFs. The SF_5^+/Xe^+ yield enhancement is significant, but not as large as with the matrix species. The analyte-to-matrix detection efficiencies are again in favor of slow ion bombardment, see Table 1. In contrast to angiotensin, however, the negative parent ion yields for chain B of insulin are roughly as high as the positive yields. The relatively high negative yields may be associated with the two SO_3H groups present in the oxidized chain B of insulin. Last but not least, the background generated under slow ion bombardment decreases rapidly at masses slightly higher than the parent ion mass. By contrast, the background induced by FFs stays at a high level even at rather high masses beyond the parent peak. This finding deserves further clarification.

Neat samples of chain B of insulin have also been prepared and analyzed at GSF. Clear parent peaks were not observed. In the negative-ion spectrum a broad hump appeared at *m/z* around 3500, superimposed on a comparatively high background.

The effect of aging and additional water treatment on the high-mass spectra of chain B of insulin is illustrated in Figure 8 for bombardment with SF_5^+. As in the matrix-dominated mass region, the peak yield decreases and the background increases upon aging. The other interesting observation is that the peaks due to doubly protonated analyte species have disappeared. Apparently aging reduces the capability of the host material to provide protons for attachment to the departing molecules. This may result from some kind of prolonged "drying" of the sample in vacuum, a process that cannot be inverted by rinsing with water. In contrast to the positive-ion mode, aging effects are small in the negative-ion mode. In fact, the peak yield in Figure 8a is even a factor of 5 higher than in Figure 7d, but the improvement must be attributed mostly to the higher extraction voltage applied to the aged sample. Rinsing with water causes a slight reduction in analyte peak height, but the peak-to-background ratios increase, not only in the negative but also in the positive mode.

Finally we present, in Figure 9, mass spectra of porcine insulin embedded in 4HCCA. The general features are similar to those observed with chain B of insulin (Figure 7). One difference is the rather low yield of negative ions for porcine insulin (no parent ions from neat samples). The other difference is the higher yield of doubly (and triply) protonated analyte molecules for porcine insulin. The fraction of doubly (and triply) protonated molecules increases in going from Xe^+ through SF_5^+ to FFs. However, it cannot be excluded that the comparatively low yield of doubly protonated parent molecules produced by slow ion impact is partly an aging effect (longer time between sample production and mass analysis than in the FF experiments). Somewhat unexpectedly, the (positive) analyte-to-matrix de-

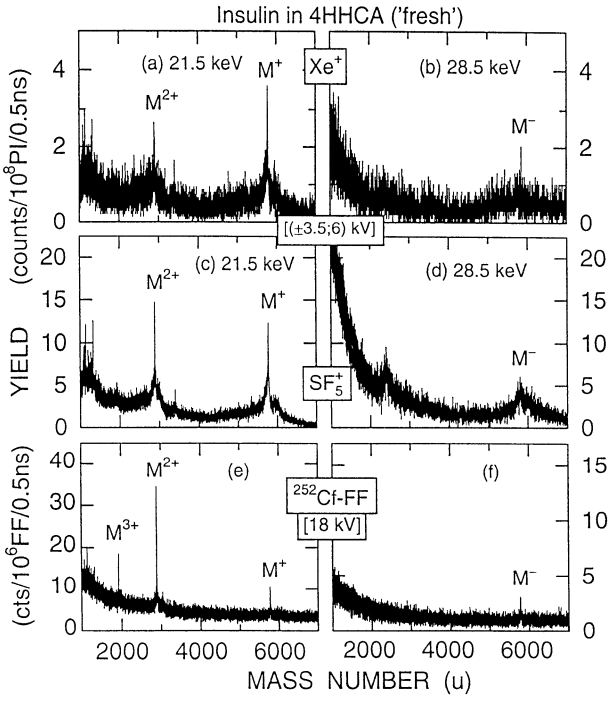

Figure 9. The same as Figure 7, but for porcine insulin in 4HCCA. 5-point smooth for all spectra.

tection efficiencies for porcine insulin are higher than for chain B of insulin, see Table 1.

Conclusions

We have shown that the concept of matrix isolation can be applied to produce intact parent ions of polypeptides by bombarding analytes embedded in 4HCCA with slow and fast primary ions. The various similarities observed with the two types of projectiles imply that the structural and chemical properties of the matrix (and the residual solvents) are the key parameters for a successful analysis. The bombardment parameters determine the absolute and relative yields of analyte and matrix ions as well as the spectrum of collisionally formed molecular ions. But, considering the large difference in energy of the ion beams and the fission fragments used in this study, the observed differences in the secondary ion spectra are relatively small. The absolute yields (per projectile) are generally decreasing in the order FF > SF_5^+ > Xe^+, but the inverse order holds true for the respective analyte-to-matrix detection efficiencies. The previously observed negative ion yield enhancement by SF_5^+ bombardment has been shown to work with samples of 4HCCA as well. The beneficial effect, however, is limited to absolute yields and does not give rise to improved analyte-to-matrix detection efficiencies. The origin of the yield enhancement still needs to be elucidated.

The results presented here strongly suggest that the low-mass region should routinely be included in the analysis of spectra obtained from matrix-embedded samples. The spectral features observed in the matrix-dominated region provide very useful information about the status of the sample and are also helpful in trying to achieve a better understanding of the energy deposition and the ion formation processes. The evaluation of aging and cleaning phenomena has thrown new light on the very important aspect of protonation. It appears that, in order to understand the protonation process, repeated measurements on the same sample must be performed as a function of storage time in vacuum. Further studies on the peaks due to intact neutral matrix molecules are highly desirable.

Probably the most exciting result of this work was the finding that the integral analyte-to-matrix detection efficiencies are very large, about 20–250 and 15–100 for protonated and deprotonated parent molecules, respectively. This effect is hard to rationalize on the basis of current understanding of ejection mechanisms in TOF-SIMS of biomolecules, unless one assumes that the efficiency for the formation of parent ions from 4HCCA is particularly poor. It is also possible that a large fraction of the analyte molecules has segregated at or near the surface during sample preparation so that the mean molar concentrations cannot be used to determine analyte-to-matrix detection efficiencies. Clearly, these very interesting aspects need to be investigated for a wider variety of material combinations.

References

1. Karas, M.; Bachmann, D.; Hillenkamp, F. *Anal. Chem.* **1985,** *57*, 2935–2939.
2. Karas, M.; Bachmann, D.; Bahr, U.; Hillenkamp, F. *Int. J. Mass Spectrom. Ion Processes* **1987,** *78*, 53–68.
3. Karas, M. *Mat. Fys. Medd. Dan Vid. Selsk.* **1993,** *43*, 623–641.
4. Bahr, U.; Karas, M.; Hillenkamp, F. *Fresenius J. Anal. Chem.* **1994,** *348*, 783–791.
5. Strupat, K.; Karas, M.; Hillenkamp, F. *Int. J. Mass Spectrom. Ion Processes* **1991,** *111*, 89–102.
6. Beavis, R. C.; Chaudhary, T.; Chait, B. T. *Org. Mass Spectrom.* **1992,** *27*, 156–158.
7. Danis, P. O.; Karr, D. E.; Mayer, F.; Holle, A.; Watson, C. H. *Org. Mass Spectrom.* **1992,** *27*, 843–846.
8. Kirpekar, F.; Nordhoff, E.; Kristiansen, K.; Roepstorff, P.; Lezius, A.; Hahner, S.; Karas, M.; Hillenkamp, F. *Nucl. Acids Res.* **1994,** *22*, 3866–3870.
9. Nelson, R. W.; Dogruel, D.; Williams, P. *Rapid Commun. Mass Spectrom.* **1995,** *9*, 625.
10. Fenselau, C. *Anal. Chem.* **1997,** *69*, 661A–665A.
11. Wu, K. J.; Odom, R. W. *Anal. Chem.* **1998,** *70*, 456A–461A.
12. Liu, L. K.; Busch, K. L.; Cooks, R. G. *Anal. Chem.* **1981,** *53*, 109–113.
13. Barber, M.; Bordoli, R. S.; Sedgwick, R. D.; Taylor, A. N. *J. Chem. Soc., Chem. Commun.* **1981**, 325.
14. Barber, M.; Bordoli, R. S.; Elliot, G. J.; Sedgwick, R. D.; Taylor, A. N. *Anal. Chem.* **1982,** *54*, 645A–657A.
15. Sundqvist, B. U. R. In *Sputtering by Particle Bombardment III*; Behrisch, R.; Wittmaack, K., Eds.; Springer: Berlin, 1991; Chap 5.
16. Aberth, W.; Straub, K. M.; Burlingame, A. L. *Anal. Chem.* **1982,** *54*, 2029–2034.
17. Cotter, R. J. *Anal. Chem.* **1984,** *56*, 2594–2596.

18. Gillen, G.; Christiansen, J. W.; Tsong, I. S. T.; Kumball, B.; Williams, P. *Rapid Commun. Mass Spectrom.* **1988,** *2*, 67–70.
19. Wolf, B.; Macfarlane, R. D. *J. Am. Soc. Mass Spectrom.* **1991,** *2*, 29–32.
20. Macfarlane, R. D.; Torgerson, D. F. *Science* **1976,** *191*, 920–925.
21. Tuszynski, W. *Int. J. Mass Spectrom. Ion Processes* **1993,** *126*, 151–156.
22. Jonsson, G. P.; Hedin, A. B.; Hakansson, P. L.; Sundqvist, B. U. R.; Säve, B. G. S.; Nielsen, P. F.; Roepstorff, P.; Johansson K.-K.; Kamensky, I.; Lindberg, M. S. L. *Anal. Chem.* **1986,** *58*, 1084–1087.
23. Metzger, J. O.; Woisch, R.; Tuszyinski, W.; Angermann, R.; Puls, J. *Rapid Commun. Mass Spectrom.* **1993,** *7*, 1041–1047.
24. Tuszynski, W.; Angermann, R.; Metzger, J. O.; Woisch, R. *Nucl. Instrum. Methods Phys. Res. B* **1994,** *88*, 184–190.
25. Metzger, J. O.; Woisch, R.; Tuszynski, W.; Angermann, R. *Fresenius J. Anal. Chem.* **1994,** *349*, 473–474.
26. Wu, K. J.; Odom, R. W. *Anal. Chem.* **1996,** *68*, 873–882.
27. Ens, W.; Standing, K. G.; Chait, B. T.; Field, F. H. *Anal. Chem.* **1981,** *53*, 1241–1244.
28. Ens, W. *Mat. Fys. Medd. Dan. Vid. Selsk.* **1993,** *43*, 155–207.
29. Szymczak, W.; Wittmaack, K. *Nucl. Instrum. Methods Phys. Res. B* **1994,** *88*, 149–153.
30. Le Beyec, Y. *Int. J. Mass Spectrom. Ion Processes* **1998,** *174*, 101–117.
31. Tuszynski, W.; Angermann, R.; Hillmann, F.; Maier-Schwartz, K. In *Ion Formation from Organic Solids*; Hedin, A.; Sundqvist, B. U. R.; Benninghoven, A., Eds.; Wiley: Chichester, 1990; pp 73–77.
32. Szymczak, W.; Wessels, J.; Kataoka, Y.; Wittmaack, K. In *Secondary Ion Mass Spectrometry SIMS XI*; Gillen, G.; Lareau, R.; Bennett, J.; Stevie, F., Eds.; Wiley: Chichester, 1998; pp 493–496.
33. Andersen, H. H. *Mat. Fys. Medd. Dan. Vid. Selsk.* **1993,** *43*, 127–153.
34. Della Negra, S.; Depauw, J.; Joret, H.; Le Beyec, Y. *Phys. Rev. Lett.* **1988,** *60*, 946–949.
35. Hilf, E. R.; Tuszynski, W.; Curdes, B.; Curdes, J.; Wagner, M.; Wien, K. *Int. J. Mass Spectrom. Ion Processes* **1993,** *126*, 101–114.
36. Wagner, M.; Wien, K.; Curdes, B.; Hilf, E. R. *Nucl. Instrum. Methods Phys. Res. B* **1993,** *82*, 362–378.
37. Betts, R. L.; da Silveira, E. F.; Schweikart, E. A. *Int. J. Mass Spectrom. Ion Processes* **1995,** *145*, 9–23.
38. Mahoney, J. F.; Perel, J.; Lee, T. D.; Martino, P. A.; Williams, P. *J. Am. Soc. Mass Spectrom.* **1992,** *3*, 311–317.
39. Biersack, J. P.; Haggmark, L. G. *Nucl. Instrum. Methods* **1980,** *174*, 257–269.